

## Electronic Supplementary Information

### Extremely High Arsenic Removal Capacity for Mesoporous Aluminium Magnesium Oxide Composites

Wei Li,<sup>‡,a</sup> Dehong Chen,<sup>b</sup> Fang Xia,<sup>a,c</sup> Jeannie Z. Y. Tan,<sup>a,b</sup> Pei-Pei Huang,<sup>d</sup> Wei-Guo Song,<sup>d</sup>

Natalita M. Nursam<sup>a,b</sup> and Rachel A. Caruso\*<sup>a,b</sup>

<sup>a</sup> CSIRO Manufacturing, Clayton South, Victoria, 3169, Australia.

<sup>b</sup> Particulate Fluids Processing Centre, School of Chemistry, The University of Melbourne, Melbourne, Victoria, 3010, Australia.

<sup>c</sup> School of Engineering and Information Technology, Murdoch University, Murdoch, West Australia, 6150, Australia.

<sup>d</sup> Beijing National Laboratory for Molecular Sciences (BNLMS), Institute of Chemistry, Chinese Academy of Sciences, Beijing, 100190, P. R. China.

<sup>‡</sup> Present address: International Iberian Nanotechnology Laboratory (INL), Avenida Mestre José Veiga, Braga, 4715-330, Portugal.

Corresponding author email: rcaruso@unimelb.edu.au

**Table S1** Physical properties of the mesoporous aluminium magnesium oxide composites calcined at 900 °C.

Sample	S <sub>BET</sub>	PSD	V <sub>sp</sub>	Phase
	[m <sup>2</sup> g <sup>-1</sup> ] <sup>a</sup>	[nm] <sup>b</sup>	[cm <sup>3</sup> g <sup>-1</sup> ] <sup>c</sup>	
meso-Al-900	172.8	10.80	0.45	γ-Al <sub>2</sub> O <sub>3</sub>
meso-90Al10Mg-900	174.9	10.84	0.47	γ-Al <sub>2</sub> O <sub>3</sub> & MgAl <sub>2</sub> O <sub>4</sub> spinel
meso-80Al20Mg-900	144.1	12.08	0.41	γ-Al <sub>2</sub> O <sub>3</sub> & MgAl <sub>2</sub> O <sub>4</sub> spinel
meso-70Al30Mg-900	91.6	13.52	0.31	γ-Al <sub>2</sub> O <sub>3</sub> & MgAl <sub>2</sub> O <sub>4</sub> spinel
meso-50Al50Mg-900	121.9	13.41	0.36	MgAl <sub>2</sub> O <sub>4</sub> spinel & cubic MgO
meso-30Al70Mg-900	101.4	8.57	0.27	MgAl <sub>2</sub> O <sub>4</sub> spinel & cubic MgO

<sup>a</sup> S<sub>BET</sub> = BET specific surface area obtained from nitrogen adsorption data in the P/P<sub>0</sub> range from 0.05 to 0.20. <sup>b</sup> PSD = pore size distribution determined by using the BJH method from the adsorption branch. <sup>c</sup> V<sub>sp</sub> = single point pore volume calculated from the adsorption isotherm at P/P<sub>0</sub> = 0.98.

**Table S2** As(V) adsorption kinetic parameters of the mesoporous aluminium magnesium oxide composites calcined at 400 °C.

Samples	Pesudo-second-order kinetic parameters		
	k [g mg <sup>-1</sup> min <sup>-1</sup> ]	q <sub>e</sub> [mg g <sup>-1</sup> ]	R <sup>2</sup>
meso-Al-400	1.02×10 <sup>-4</sup>	147.71	0.999
meso-90Al10Mg-400	9.25×10 <sup>-5</sup>	125.63	0.996
meso-80Al20Mg-400	7.14×10 <sup>-5</sup>	178.57	0.998
meso-70Al30Mg-400	5.20×10 <sup>-5</sup>	181.82	0.996
meso-50Al50Mg-400	5.76×10 <sup>-5</sup>	165.84	0.998
meso-30Al70Mg-400	2.67×10 <sup>-4</sup>	74.52	0.998
meso-Mg-400	1.62×10 <sup>-4</sup>	207.90	0.999
Al-400	1.35×10 <sup>-4</sup>	17.30	0.897

**Table S3** As(V) adsorption isotherm parameters of the mesoporous aluminium magnesium oxide composites calcined at 400 °C.

Sample	Highest adsorption capacity [mg g <sup>-1</sup> ] <sup>a</sup>	Langmuir isotherm			Freundlich isotherm		
		q <sub>m</sub> [mg g <sup>-1</sup> ]	b	R <sup>2</sup>	K <sub>F</sub>	1/n	R <sup>2</sup>
meso-Al-400	299.03	271.83	0.4057	0.9716	94.55	0.1806	0.8621
meso-90Al10Mg-400	430.92	333.29	0.2536	0.8485	100.43	0.2100	0.9437
meso-80Al20Mg-400	502.97	422.09	0.0590	0.8902	95.85	0.2456	0.9795
meso-70Al30Mg-400	487.56	438.80	0.0321	0.8916	89.69	0.2531	0.9838
meso-50Al50Mg-400	466.02	416.25	0.0292	0.8778	86.18	0.2486	0.9730
meso-30Al70Mg-400	396.06	587.45	0.0022	0.8630	18.33	0.4482	0.9212
meso-Mg-400	912.32	928.95	0.1296	0.9692	242.32	0.2346	0.8059
Al-400	72.20	72.48	0.0259	0.9120	15.42	0.2362	0.9635

<sup>a</sup> The highest adsorption capacity was achieved using an initial arsenic concentration of 1020 mg L<sup>-1</sup>.

**Table S4** As(V) adsorption isotherm parameters of the mesoporous aluminium magnesium oxide composites calcined at 900 °C.

Sample	Highest adsorption capacity [mg g <sup>-1</sup> ] <sup>a</sup>	Langmuir isotherm			Freundlich isotherm		
		q <sub>m</sub> [mg g <sup>-1</sup> ]	b	R <sup>2</sup>	K <sub>F</sub>	1/n	R <sup>2</sup>
meso-Al-900	79.21	76.36	0.5496	0.9748	38.29	0.1203	0.8421
meso-90Al10Mg-900	92.61	87.76	1.9477	0.9732	46.58	0.1134	0.8331
meso-80Al20Mg-900	70.94	58.45	1.4830	0.9254	32.65	0.1090	0.9206
meso-70Al30Mg-900	43.78	35.42	0.7144	0.8900	20.10	0.1036	0.8942
meso-50Al50Mg-900	97.56	91.32	0.5279	0.8189	46.71	0.1163	0.7739
meso-30Al70Mg-900	165.85	159.01	1.079	0.9087	71.23	0.1397	0.7750

<sup>a</sup> The highest adsorption capacity was achieved using an initial arsenic concentration of 1020 mg L<sup>-1</sup>.

**Table S5** As(III) adsorption isotherm parameters of the mesoporous aluminium magnesium oxide composites calcined at 400 °C.

Sample	Highest adsorption capacity [mg g <sup>-1</sup> ] <sup>a</sup>	Langmuir isotherm			Freundlich isotherm		
		q <sub>m</sub> [mg g <sup>-1</sup> ]	b	R <sup>2</sup>	K <sub>F</sub>	1/n	R <sup>2</sup>
meso-Al-400	114.85	120.49	0.1091	0.9815	15.37	0.3171	0.9497
meso-90Al10Mg-400	143.12	157.58	0.0192	0.9901	18.10	0.3336	0.8784
meso-80Al20Mg-400	390.59	424.26	0.0011	0.9320	2.19	0.8137	0.9861
meso-70Al30Mg-400	330.58	416.24	0.0018	0.9452	3.21	0.7288	0.9720
meso-50Al50Mg-400	240.78	394.71	0.0022	0.9919	4.18	0.6243	0.9918
meso-30Al70Mg-400	120.39	196.06	0.0019	0.9731	1.91	0.6264	0.9694
meso-Mg-400	812.84	848.72	0.1007	0.9214	162.8	0.2945	0.7509

<sup>a</sup> The highest adsorption capacity was achieved using an initial arsenic concentration of 820 mg L<sup>-1</sup>.

**Table S6** Atomic ratios of the mesoporous aluminium magnesium oxide composites calcined at 400 °C before and after adsorption of 400 mg L<sup>-1</sup> of As(V) at pH 3.0 or As(III) at pH 7.0 obtained from XPS analysis.

Sample	Atomic ratio			
	Al	Mg	Al/Mg	As
meso-Al-400	16.07	0		0
As(V)-meso-Al-400	25.85	0		4.61
As(III)-meso-Al-400	17.27	0		2.23
Meso-80Al20Mg-400	1.37	6.22	4.54	0
As(V)-meso-80Al20Mg-400	10.31	1.11	9.29	3.07
As(III)-meso-80Al20Mg-400	17.06	1.72	9.92	4.41
meso-Mg-400	0	10.39		0
As(V)-meso-Mg-400	0	20.6		5.9
As(III)-meso-Mg-400	0	13.86		3.38

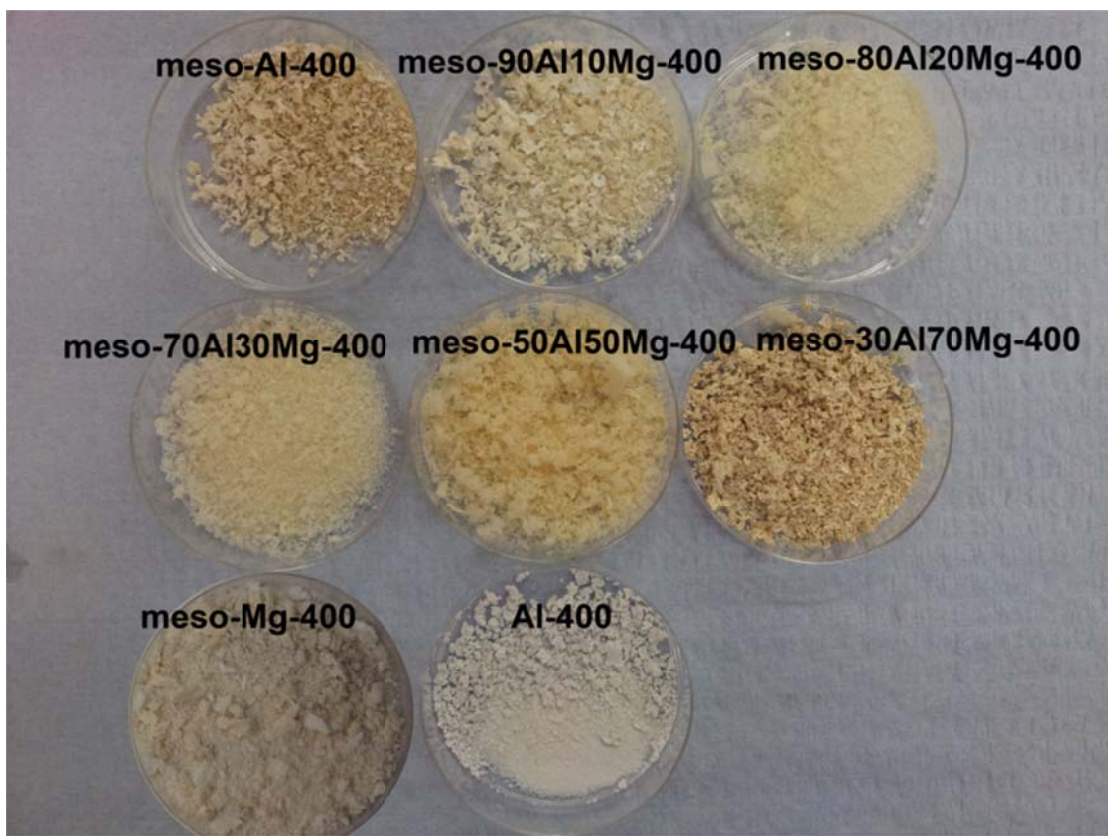


**Figure S1** A photograph of the as-prepared mesoporous aluminium magnesium oxides calcined at 400 °C.

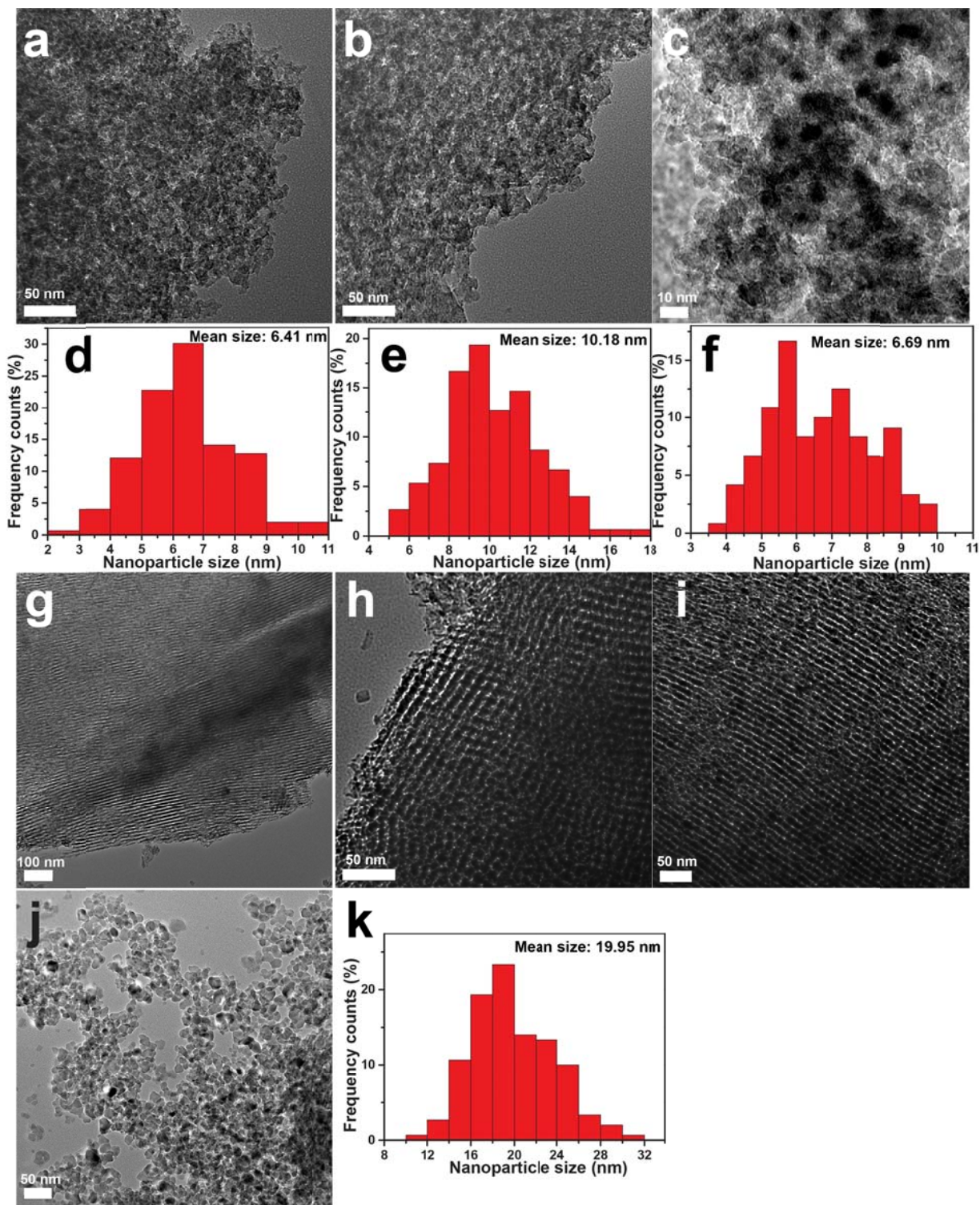


**Figure S2** TEM images of (a) meso-50Al50Mg-400, (b) meso-30Al70Mg-400 and (c) meso-Mg-400. Particle size distribution of (d) meso-50Al50Mg-400, (e) meso-30Al70Mg-400 and (f) meso-Mg-400. TEM images of (g) meso-Al-900, (h) meso-90Al10Mg-900, (i) meso-80Al20Mg-900, (j) meso-70Al30Mg-900 and particle size distribution of (k) meso-70Al30Mg-900. Over 150 nanoparticles were analyzed for particle size distribution statistics by using software Nanomeasure 1.25 and Origin 9.0.

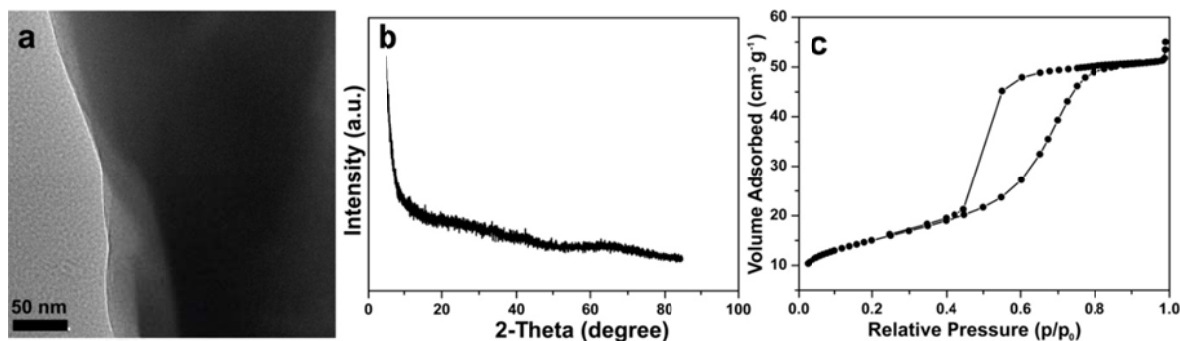


**Figure S3** TEM image (a), XRD pattern (b) and the nitrogen gas sorption isotherm (c) of the control sample Al-400 synthesized in the absence of the P123 soft template.

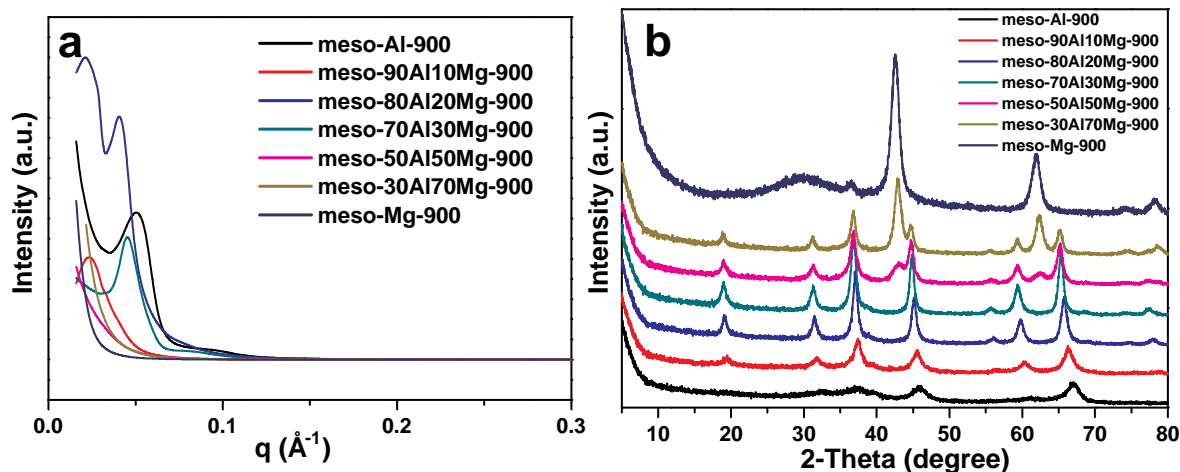


**Figure S4** (a) Synchrotron SAXS and (b) wide angle XRD patterns of mesoporous aluminium magnesium oxide samples with varying Mg/Al molar ratios calcined at 900 °C.

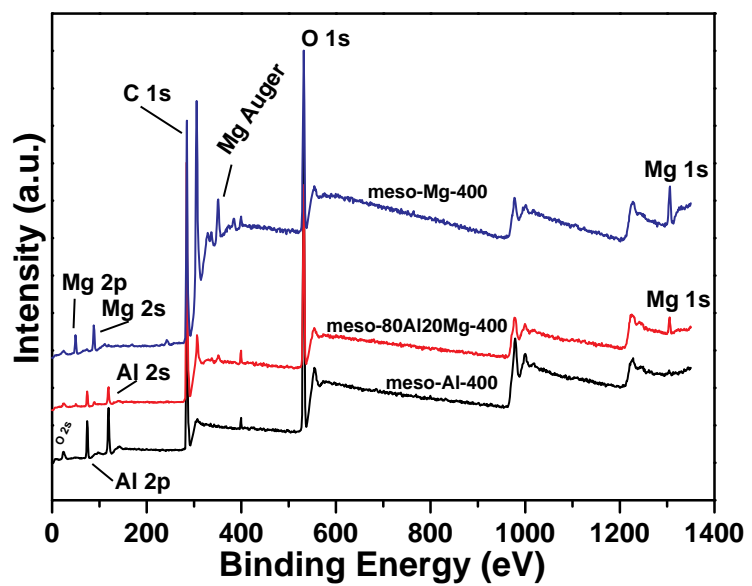


**Figure S5** The full XPS survey of meso-Al-400, meso-80Al20Mg-400 and meso-Mg-400.

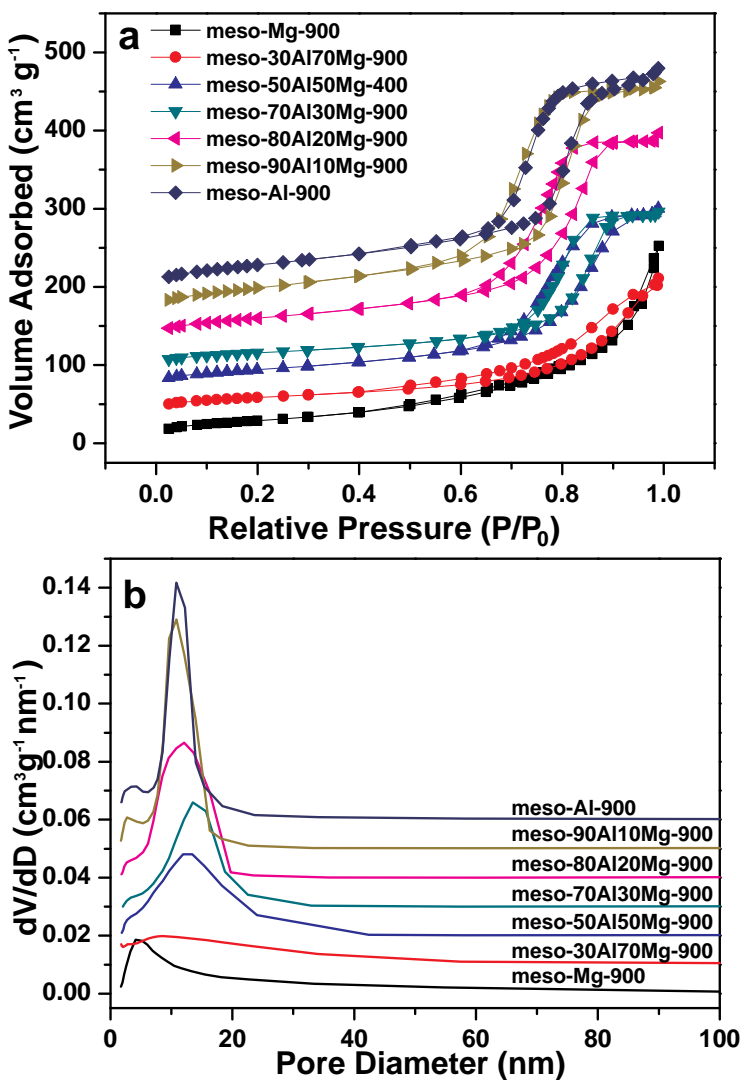


**Figure S6** Nitrogen gas sorption isotherms of the mesoporous aluminium magnesium oxides with varying Mg/Al molar ratios calcined at 900 °C and (b) the corresponding pore size distribution derived from the adsorption branches based on the BJH model. Each subsequent curve is shifted up the y axis by  $30 \text{ cm}^3 \text{ g}^{-1}$  in (a) and  $0.01 \text{ cm}^3 \text{ g}^{-1} \text{ nm}^{-1}$  in (b), for clarity.

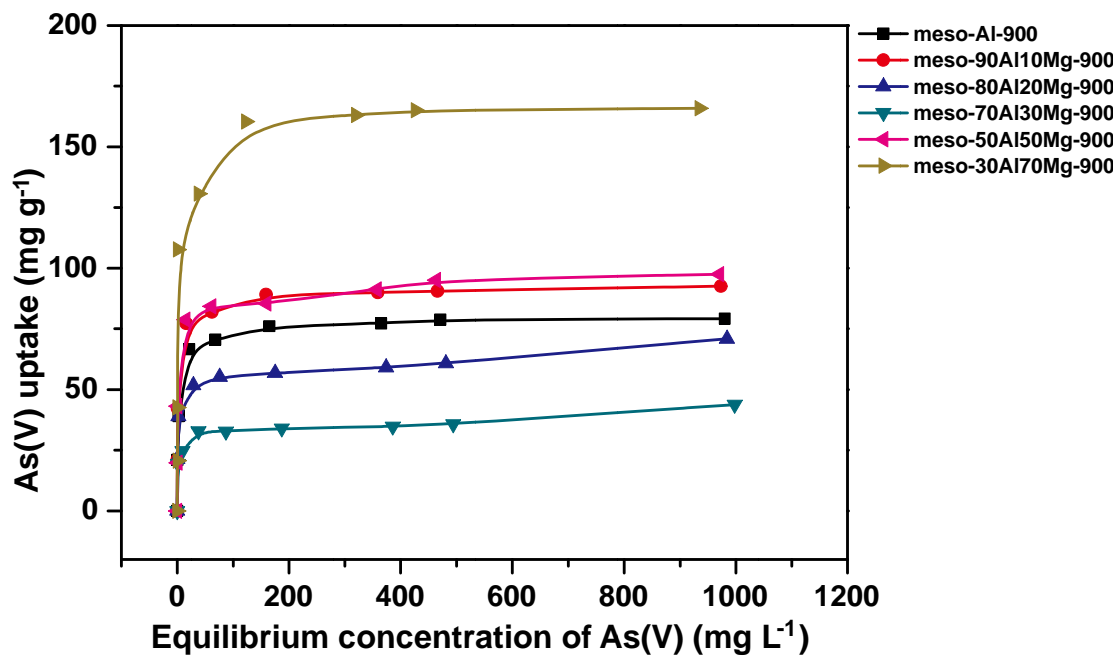


**Figure S7** Adsorption isotherms of As(V) on mesoporous aluminium magnesium oxides with varying Mg/Al molar ratios calcined at 900 °C. Experimental conditions: dose = 0.5 g L<sup>-1</sup>, initial pH = 3.0, the initial As(V) concentration ranged from 10 to 1000 mg L<sup>-1</sup>.

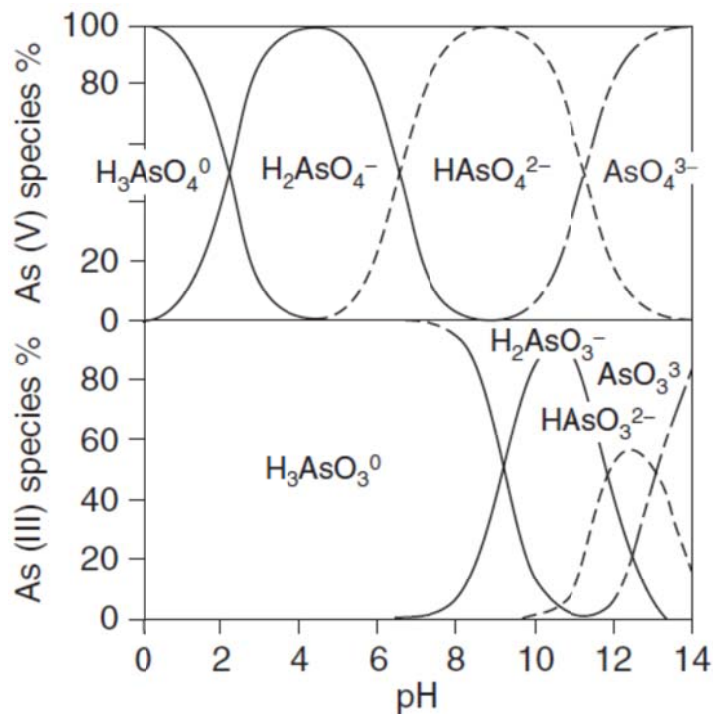


**Figure S8** Distribution of As(V) and As(III) species under different pH values. Reproduced with permission [P. Ravenscroft, H. Brammer, K. Richards, *Arsenic Pollution: A Global Synthesis*, Wiley-Blackwell, USA 2009, pp. 25]. Copyright 2009, John Wiley & Sons.

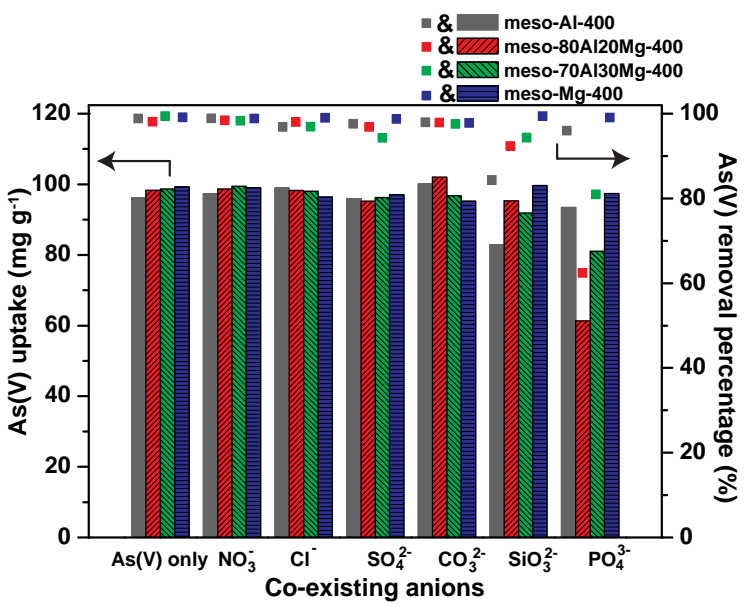


**Figure S9** Effect of co-existing anions on the adsorption capacities of meso-Al-400, meso-80Al20Mg-400, meso-70Al30Mg-400 and meso-Mg-400 for As(V). Experimental conditions: dose = 0.5 g L<sup>-1</sup>, initial pH = 6.0, initial As(V) concentration = 50 mg L<sup>-1</sup>; initial concentration of co-existing anions: 10 mg L<sup>-1</sup> of  $\text{NO}_3^-$ , 200 mg L<sup>-1</sup> of  $\text{Cl}^-$ , 200 mg L<sup>-1</sup> of  $\text{SO}_4^{2-}$ , 50 mg L<sup>-1</sup> of  $\text{CO}_3^{2-}$ , 50 mg L<sup>-1</sup> of  $\text{SiO}_3^{2-}$  or 50 mg L<sup>-1</sup> of  $\text{PO}_4^{3-}$ .

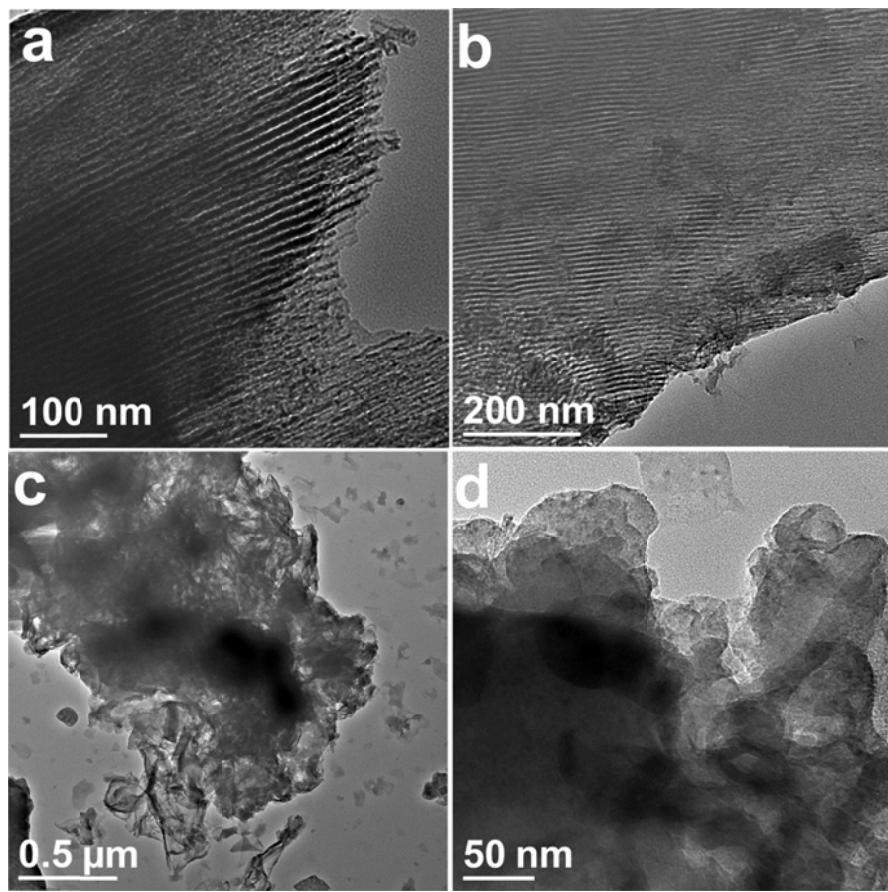


**Figure S10** TEM images of (a) meso-Al-400, (b) meso-80Al20Mg-400, (c) and (d) meso-Mg-400 after adsorption of 400 mg L<sup>-1</sup> of As(V) solution at an initial pH of 3.0.

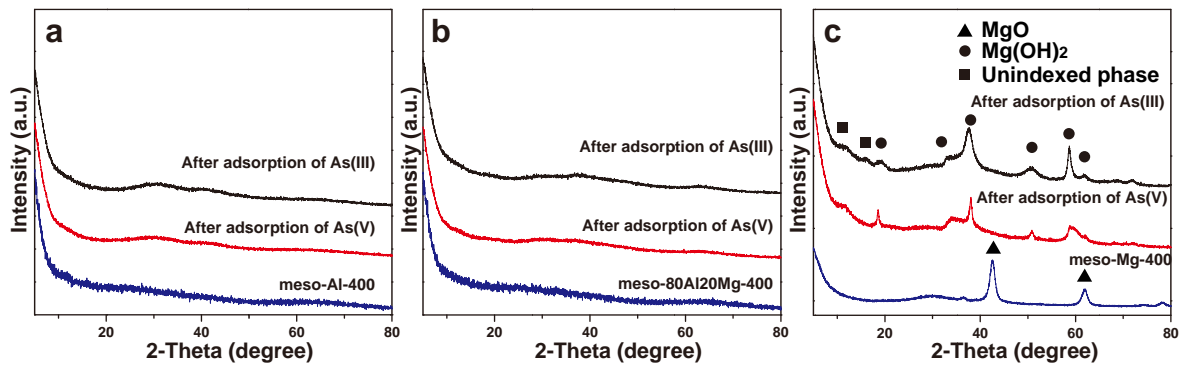


**Figure S11** XRD patterns of the adsorbents before and after adsorption of 400 mg L<sup>-1</sup> of As(V) and As(III) at the initial pH of 3.0 and 7.0, respectively: (a) meso-Al-400, (b) meso-80Al20Mg-400 and (c) meso-Mg-400.

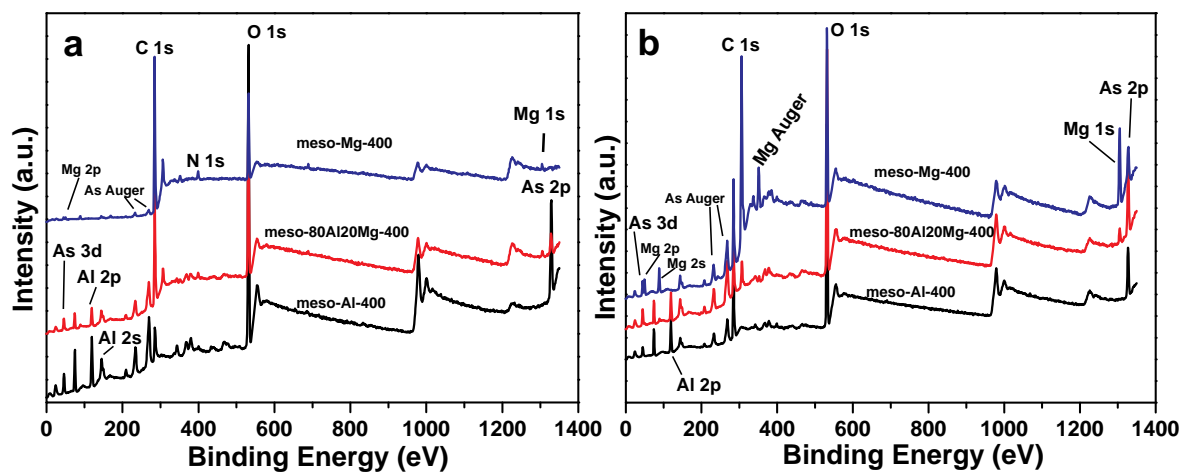


**Figure S12** The full XPS survey of meso-Al-400, meso-80Al20Mg-400 and meso-Mg-400 after adsorption of 400 mg L<sup>-1</sup> of (a) As(V) and (b) As(III). Experimental conditions: dose = 0.5 g L<sup>-1</sup>, initial pH for As(V) and As(III) adsorption is 3.0 and 7.0, respectively.

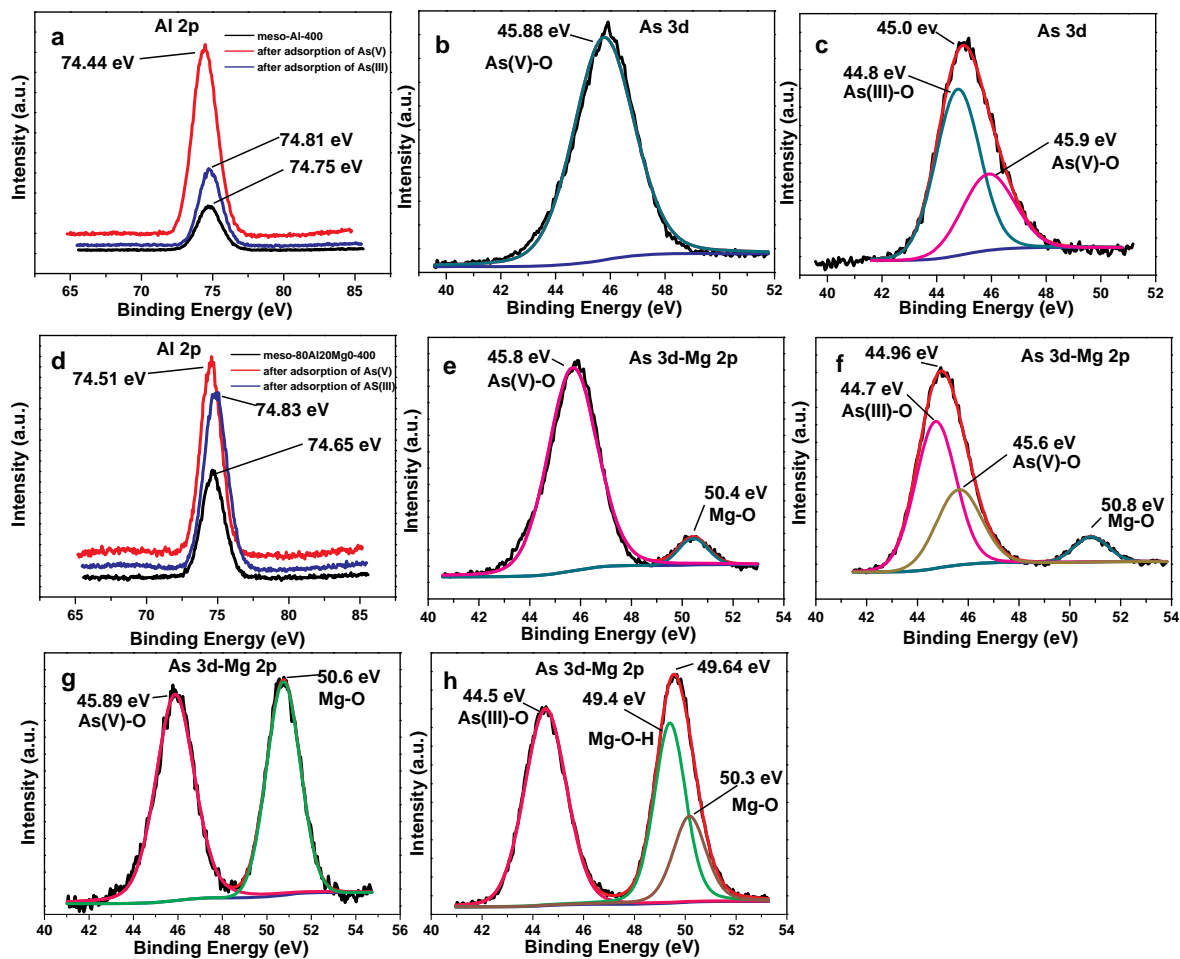


**Figure S13** (a) Al 2p XPS peak of meso-Al-400 before and adsorption of As(V) and As(III), (b) As 3d peak of meso-Al-400 after adsorption of As(V), (c) As 3d peak of meso-Al-400 after adsorption of As(III), (d) Al 2p XPS peak of meso-80Al20Mg-400 before and after adsorption of As(V) and As(III), (e) As 3d and Mg 2p peak of meso-80Al20Mg-400 after adsorption of As(V), (f) As 3d and Mg 2p peak of meso-80Al20Mg-400 after adsorption of As(III), (g) and (h) As 3d and Mg 2p peak of meso-Mg-400 after adsorption of As(V) and As(III), respectively. Experimental conditions: dose = 0.5 g L<sup>-1</sup>, initial concentration of As(V) or As(III) = 400 mg L<sup>-1</sup>; initial pH for As(V) and As(III) adsorption is 3.0 and 7.0, respectively.

As shown in Figure S13a and d, for both meso-Al-400 and meso-80Al20Mg-400, the Al 2p peak shifts towards lower binding energy after adsorption of As(V), while the Al 2p peak moves slightly towards higher binding energy after As(III) adsorption. This difference in the Al 2p peak shift after adsorption of As(V) or As(III) over meso-Al-400 and meso-80Al20Mg-400 is likely to be due to the following reasons:

1. The initial pH is different for adsorption of As(V) or As(III) over the samples for the XPS measurement. In this work, the initial pH for As(V) and As(III) adsorption on both meso-Al-400

and meso-80Al20Mg-400 is 3.0 and 7.0, respectively. The initial pH affects the different dominant arsenic speciation, As(V) ( $\text{H}_2\text{AsO}_4^-$ ) and As(III) ( $\text{H}_3\text{AsO}_3^0$ ), which in turn caused the different shift of the Al 2p peak when forming Al-O-As bonds during the XPS measurement.

2. There are various models of surface complexes for the arsenic (including As(V) and As(III)) immobilization on aluminium oxy-hydroxides and other metal hydroxides/oxides. Most publications proved that arsenic can be adsorbed onto variable-charge adsorbent surfaces by inner-sphere complexation (ligand exchange to form chemical bonding) and/or outer-sphere complexation (electrostatic interaction or hydrogen bonding)(*Geoderma* 2001, 100, 303–319). The type of sorption mechanism for a particular ion is greatly affected by environmental factors such as pH and ionic strength.

For the inner-sphere surface complex, there are four molecular configurations including bidentate binuclear, bidentate mononuclear, monodentate binuclear and monodentate mononuclear (*Geochimica et Cosmochimica Acta* 2012, 83, 205–216; *Geochimica et Cosmochimica Acta* 2001, 65, 1211–1217). For each configuration, acid-base or non-dissociative sorption could be included (*Journal of Molecular Structure: THEOCHEM* 2006, 762, 17–23; *Geochimica et Cosmochimica Acta* 2012, 83, 205–216). The specific mechanism would be elucidated by X-ray absorption spectroscopy (XAS) including EXAFS and XANES. Generally, the adsorption mechanism is considered to be different for As(V) or As(III) immobilized on the aluminium oxides, although there is no consensus on the exact mechanism applied for either As(V) or As(III).

Most publications reported that As(V) predominantly forms inner-sphere bidentate binuclear complexes with the surface of aluminium oxide (*Chemosphere* 2004, 55, 1259–1270; *Journal of Colloid and Interface Science* 2001, 234, 204–216; *Environmental Science & Technology* 2005, 39, 5481–5487; *Environmental Toxicology and Chemistry* 2006, 25, 3118–3124; *Journal of Colloid and Interface Science* 2001, 235, 80–88; *Applied Geochemistry* 2013, 31, 79–83; *Environmental Science & Technology* 2011, 45, 9687–9692), while some papers claimed the inner-sphere monodentate mononuclear complexes (*Environmental Science & Technology* 2009, 43, 2537–2543) and co-existing inner-sphere, hydrogen bond and electrostatic interactions would dominate depending on the pH (*Journal of Hazardous Materials* 254–255 (2013) 301–309; *Environmental Science & Technology* 2006, 40, 7784–7789; *Environmental Science & Technology* 2005, 39, 3571–3579; *Microporous and Mesoporous Materials* 2014, 198, 101–114; *Geochimica et Cosmochimica Acta* 2008, 72, 1986–2004).

The dominant complexes debated for As(III)-aluminium oxide surface complexation including outer-sphere (*Chemosphere* 2003, 51, 1001–1013; *Journal of Colloid and Interface Science* 2001, 234, 204–216; *Soil Science Society of America Journal* 70:2017–2027; *Environmental Chemistry Letters* 2013, 11, 289–294), non-dissociative inner-sphere complexes (*Journal of Molecular*

Structure: THEOCHEM 2006, 762, 17–23), inner-sphere bidentate binuclear (*Geochimica et Cosmochimica Acta* 2012, 83, 205–216; *Microporous and Mesoporous Materials* 2014, 198, 101–114), a combination of inner-sphere bidentate binuclear and bidentate mononuclear (*Chemosphere* 2014, 113, 151–157), as well as co-existing mixtures of several surface inner-sphere complexes and outer-sphere complexes (*Journal of Colloid and Interface Science* 2001, 235, 80–88).

Because of the different kinds of surface complexes obtained through chemical bonding (inner-sphere configurations) and possible discernable intervention from electrostatic outer-sphere complexes, the XPS peak shift is likely different between As(V) at pH 3.0 and As(III) at pH 7.0, even if the As(V) and As(III) species are chemisorbed onto the surface of meso-Al-400 and meso-80Al20Mg-400 forming As-O-M bonds. The different kinds of surface complexes have been reported to cause either a positive or negative Al 2p peak shift in the Fe/Al hydroxide when adsorbing different speciations of As(V), indicating that the Al 2p peak shift is not necessarily consistent even though an As-O-Al bond is formed. (*Journal of Hazardous Materials* 2015, 293, 97–104)

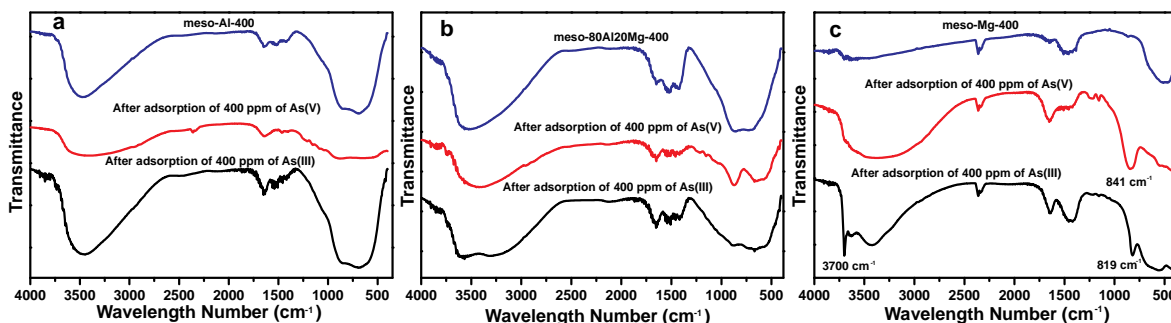


**Figure S14** FTIR spectra of the vacuum-dried samples before and after adsorption of arsenic: (a) meso-Al-400, (b) meso-80Al20Mg-400 and (c) meso-Mg-400. Experimental conditions: dose = 0.5 g L<sup>-1</sup>, initial concentration of As(V) or As(III) = 400 mg L<sup>-1</sup>; initial pH for As(V) and As(III) adsorption is 3.0 and 7.0, respectively.

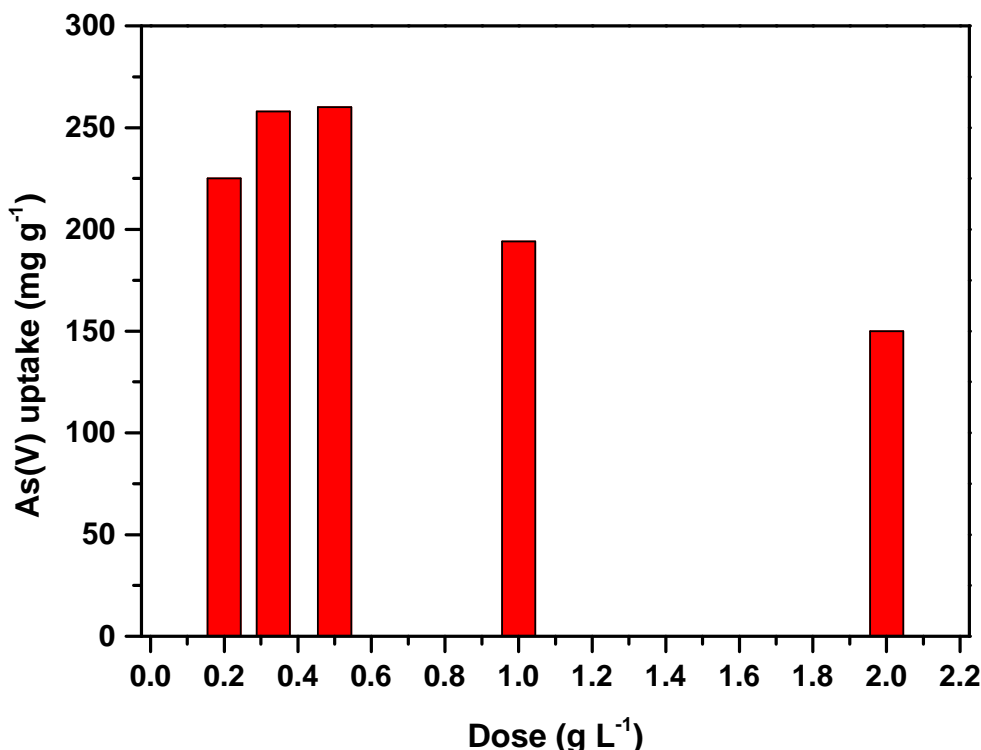


**Figure S15** Effect of the adsorbent dose on the As(V) adsorption capacity of meso-Al-400. The mass of meso-Al-400 was 0.02 g, the initial pH was  $3.0 \pm 0.1$  and the initial As(V) concentration is  $420 \text{ mg L}^{-1}$ . The volume of As(V) solution was varied from 10 to 100 mL, resulting in the dose ranging from  $0.2 \text{ g L}^{-1}$  to  $2.0 \text{ g L}^{-1}$ .

Please note that the adsorbent dose was  $0.5 \text{ g L}^{-1}$  throughout the work. Figure S15 demonstrates that  $0.5 \text{ g L}^{-1}$  is the optimal adsorbent dose with the highest adsorption capacity ( $260 \text{ mg g}^{-1}$ ) for As(V). When the dose was increased to  $1.0$  and  $2.0 \text{ g L}^{-1}$ , the adsorption capacity was decreased by 25.4% and 42.3%, respectively.